Available online at www.sciencedirect.com
ScienceDirect
International Journal of Heat and Mass Transfer 51 (2008) 4139–4144
International Journal of HEAT and MASS TRANSFER
www.elsevier.com/locate/ijhmt

Technical Note

Burnett simulation of gas flow and heat transfer in micro Poiseuille flow

Fubing Bao [a,b], Jianzhong Lin [a,b,*]

[a] Department of Mechanics, State Key Laboratory of Fluid Power Transmission and Control, Zhejiang University, Hangzhou 310027, China
[b] China Jiliang University, Hangzhou 310018, China

Received 13 June 2007; received in revised form 16 November 2007
Available online 9 May 2008

Abstract

The Burnett equations with slip boundary conditions are used to simulate the compressible gas flow and heat transfer in micro Poiseuille flow in the slip and transition flow regime. A relaxation method on Burnett terms is proposed in the present study and the thermal creep effect is considered. Convergent results at Knudsen number up to 0.4 are achieved and the results agree very well with experimental data. It is found that with the increase of Knudsen number, the Poiseuille number decreases while Nusselt number increases. The local Poiseuille number decreases along the whole channel while the local Nusselt number decreases rapidly first and then increases slowly afterwards.

Keywords: Burnett equations; Heat transfer; Slip boundary condition; Poiseuille flow; Thermal creep effect

1. Introduction

Research interest on gas flow and heat transfer phenomena in microchannels has increased substantially in recent years due to the developments in the electronic industry, microfabrication technologies, biomedical engineering, etc. Microscale fluid flow and heat transfer behaviors differ greatly from those at macroscale [1–3]. Experiments conducted by Harley et al. [1] on low Reynolds number gas flows in microchannels showed that conventional analyses are unable to predict the observed flow rates with any degree of accuracy.

The direct simulation Monte Carlo (DSMC) method has achieved great success in modeling the rarefied gas flow [4]. But this method requires a large number of particles for accurate simulation and is very expensive both in computational time and memory requirements, especially for the low-speed flow in micro electro mechanical systems (MEMS) and nanodevices [4].

As an alternative, higher-order extended or generalized hydrodynamic equations have been proposed that can perform well in both the continuum and slip–transition regimes [2,3]. Higher-order constitutive relations, beyond the Navier–Stokes equations, for stress and heat transfer terms are obtained using the Chapman–Enskog expansion of the Boltzmann equation with *Kn* as a parameter [5]. Among them, the Burnett equations have been a subject of considerable investigation in recent years. They were firstly used to model the shock wave in the transition regime and it was found that the Burnett equations provide much more accurate numerical solutions than the Navier–Stokes equations [3,6]. Recently, the Burnett equations were also used to simulate the gas flow and heat transfer in small devices in slip and transition flows. The Couette flow and Poiseuille between two parallel plates were simulated and compared with Naveir–Stokes results. Burnett results show better agreement with DSMC results than those of the Navier–Stokes equations [3,7,8].

Heat transfer characters in microchannels have been studied by many researchers. Aydin and Avci [9] investigated analytically the laminar heat transfer in micro

* Corresponding author. Address: Department of Mechanics, State Key Laboratory of Fluid Power Transmission and Control, Zhejiang University, Hangzhou 310027, China. Tel.: +86 571 8795 2882; fax: +86 571 8795 1464.
E-mail address: mecjzlin@public.zju.edu.cn (J. Lin).

0017-9310/$ - see front matter © 2008 Elsevier Ltd. All rights reserved.
doi:10.1016/j.ijheatmasstransfer.2007.12.009

Nomenclature

e_t	total energy
f	friction factor
H	height of channel, m
Kn	Knudsen number
L	length of channel, m
Nu	Nusselt number (hH/κ)
p	pressure, Pa
Po	Poiseuille number ($Po = fRe$)
Pr	Prandtl number ($Pr = \nu/\alpha$)
q_i	heat flux vector
R	gas constant, J/(kg K)
Re	Reynolds number ($Re = \rho H u_m/\mu$)
R_f	relaxation factor
T	temperature, K
u, v, w	velocity components, m/s

Greek symbols

γ	specific heat ratio
λ	molecular mean free path, m
μ	dynamic viscosity, kg/(m s)
Π	pressure ratio ($\Pi = p_i/p_o$)
ρ	density, kg/m^3
σ_{ij}	viscous stress tensor
σ_T	thermal accommodation coefficient
σ_v	tangential moment accommodation coefficient

Subscripts or superscripts

grid	value based on grid
i	inlet value
L	local value
new	value after relaxation
o	outlet value
old	value of previous iteration
s	fluid property at the wall
w	wall value
λ	value at mean free path away from the wall

Poiseuille flow. Hadjiconstantinou and Simek [10] studied the constant wall temperature problem in 2-D micro and nano channels in the slip and transition regimes. Renksizhulut et al. [11] investigated numerically the rarefied gas flow and heat transfer in the entrance region of rectangular microchannels in the slip flow regime. It is found that the temperature jump effect is very important and neglecting of this effect leads to a significant over prediction of heat transfer rate.

But in all the above studies, the compressibility of the gas is neglected. The compressible effect is very important in microchannel flow [3,11–13]. Neglecting of compressibility is not appropriate, especially under large pressure ratio. Guo and Wu [12] investigated the compressibility and rarefied effects in microchannel and concluded that the compressibility is important and should be considered. Asako et al. [13] solved two dimensional compressible momentum and energy equations to obtain the effect of compressibility on gaseous flow characteristics in microchannels. Chen [14] investigated the heat transfer characteristics of compressible flow in microchannels, but non-slip boundary conditions are used in their simulations.

A relaxation method is proposed in the present study. By using this relaxation method, convergent results of Burnett equations at Kn up to 0.4 was achieved. Even though Lockerby and Reese [15] have successfully extended numerical simulation to Kn exceeding 1. They only solved one dimensional Burnett equations. When the same method was used to the two dimensional Poiseuille flow, convergent solution can only be reached at Kn up to 0.2. Burnett equations are then used to study the compressible gaseous flow and heat transfer characteristics in microfluidic and nanofluidic systems.

2. Burnett equations

The Burnett equations are the second-order approximation of the Chapman–Enskog solution to the Boltzmann equation. The Augmented Burnett equations are widely used in previous studies [3,13] and they are adopted in the present study. The governing equations of two dimensional unsteady compressible viscous flow can be written in Cartesian coordinates as

$$\frac{\partial \mathbf{Q}}{\partial t} + \frac{\partial \mathbf{E}}{\partial x} + \frac{\partial \mathbf{F}}{\partial y} = 0, \tag{1}$$

where

$$\mathbf{Q} = \begin{bmatrix} \rho \\ \rho u \\ \rho v \\ e_t \end{bmatrix}, \quad \mathbf{E} = \begin{bmatrix} \rho u \\ \rho u^2 + p + \sigma_{11} \\ \rho uv + \sigma_{12} \\ (e_t + p)u + \sigma_{11}u + \sigma_{12}v + q_1 \end{bmatrix},$$

$$\mathbf{F} = \begin{bmatrix} \rho v \\ \rho uv + \sigma_{21} \\ \rho v^2 + p + \sigma_{22} \\ (e_t + p)v + \sigma_{21}u + \sigma_{22}v + q_2 \end{bmatrix}.$$

The viscous stress tensor σ_{11} can be expressed as follows:

$$\begin{aligned}\sigma_{11} = &-\mu\left(\frac{4}{3}u_x - \frac{2}{3}v_y\right) + \frac{\mu^2}{p}\left(\alpha_1 u_x^2 + \alpha_2 u_y^2 + \alpha_3 v_x^2 + \alpha_4 v_y^2\right.\\ &+\alpha_5 u_x v_y + \alpha_6 u_y v_x + \alpha_7 RT_{xx} + \alpha_8 RT_{yy} + \alpha_9 \frac{RT}{\rho}\rho_{xx}\\ &+\alpha_{10}\frac{RT}{\rho}\rho_{yy} + \alpha_{11}\frac{RT}{\rho^2}\rho_x^2 + \alpha_{12}\frac{RT}{\rho^2}\rho_y^2 + \alpha_{13}\frac{R}{T}T_x^2\\ &\left.+\alpha_{14}\frac{R}{T}T_y^2 + \alpha_{15}\frac{R}{\rho}T_x\rho_x + \alpha_{16}\frac{R}{\rho}T_y\rho_y\right)\\ &+\frac{\mu^3}{p^2}RT(\alpha_{17}u_{xxx} + \alpha_{17}u_{xyy} + \alpha_{18}v_{xxy} + \alpha_{18}v_{yyy}) \end{aligned} \tag{2}$$

The other viscous stress tensor σ_{ij} and heat flux vector q_i are omitted here because of the space limit. Please refer to [3] for more information about the equations. Here the Sutherland's law is adopted to modify viscosity.

The pressure obeys the perfect gas law

$$p = \rho RT. \tag{3}$$

Eqs. (1) and (3) form a set of closed equations and ρ, u, v, T, p can be solved with appropriate boundary conditions.

3. Slip boundary conditions

Non-slip boundary conditions are generally unrealistic for slip and transition flows as there are not enough collisions near the wall to equilibrate the flow field. The classical slip boundary conditions of this type are the Maxwell–Smoluchowski first-order slip conditions:

$$u_s - u_w = \frac{2-\sigma_v}{\sigma_v}\lambda\left.\frac{du}{dy}\right|_w + \frac{3}{4}\frac{\mu}{\rho T}\left.\frac{\partial T}{\partial x}\right|_w, \tag{4a}$$

$$T_s - T_w = \frac{2-\sigma_T}{\sigma_T}\frac{2\gamma}{Pr(\gamma+1)}\lambda\left.\frac{dT}{dy}\right|_w. \tag{4b}$$

The second term on the right of Eq. (4b) is thermal creep contribution to slip velocity. Analytical models derived using the first-order slip boundary condition have been shown to be relatively accurate up to Kn of approximately 0.1 [1]. For $Kn > 0.1$, however, experimental studies have shown that models based on the first-order boundary condition show considerable discrepancies against observed data [16]. Different kinds of second-order slip boundary conditions are studied, but no consensus has been reached on the correct form of second-order formulation [17].

In the present study, a general slip boundary condition proposed by Beskok et al. [18] is adopted.

$$u_s = \frac{1}{2}[u_\lambda - (1-\sigma_v)u_\lambda + \sigma_v u_w] + \frac{3}{4}\frac{\mu}{\rho T}\left.\frac{\partial T}{\partial x}\right|_w. \tag{5a}$$

$$T_s = \frac{\frac{2-\sigma_T}{Pr}\frac{\gamma}{\gamma+1}T_\lambda + \sigma_T T_w}{\sigma_T + \frac{2-\sigma_T}{Pr}\frac{\gamma}{\gamma+1}}. \tag{5b}$$

where T_λ means the temperature at a mean free path away from the wall. This kind of slip boundary condition corresponds to a high-order slip boundary condition by simply expanding u_λ in terms of u_s, using Taylor series expansion.

4. Numerical algorithm

The schematic of pressure-driven microchannel flow is shown in Fig. 1. The flow is driven by the pressure difference between the inlet pressure and outlet pressure. The ratio of these two pressures is defined as Π.

The Burnett equations are hard to converge. As mentioned by many researchers, the Burnett equations are unstable at fine grids [19,20]. Very coarse grids were used in their simulations to get convergent results. Convergent results can only be achieved at Kn up to 0.2. A relaxation method is proposed in the present simulation. The relaxation factor, R_f, is used to compute the augmented Burnett value of the new iteration as follows:

$$B_{new} = B_{old} + R_f(B - B_{old}), \tag{6}$$

where B denotes the third term on the right of Eq. (2). By using this relaxation method in the augmented Burnett terms, the computation is more likely to converge. Different values of relaxation factor are examined and we find that with a relaxation value of 0.01, the convergent results of the Burnett equations can be achieved up to $Kn = 0.4$, using 20 grids in the direction normal to the wall.

The numerical instability of the Burnett equations are associated with the grid Knudsen number, which can be defined based on the grid dimension

$$Kn_{grid} = \frac{\lambda}{\min(\Delta x, \Delta y)}, \tag{7}$$

where Δx and Δy are grid sizes in the x and y direction, respectively. According to our computation, the critical Kn_{grid} is about 8. When Kn_{grid} is larger than this value, the computation becomes unstable.

The present computation is based on SIMPLE algorithm. A grid dependence test is first carried out for the nitrogen flow in a 40 μm × 2 μm microchannel. The central difference interpolation was adopted here. The inlet and outlet pressure are 150 and 100 kPa, respectively. So the inlet to outlet pressure ratio is 1.5. The temperature of inlet gas is 300 K. Isentropic relations for an ideal gas are applied to calculate the inlet velocity. The temperature and velocity at outlet are extrapolated from the interior of the domain. Five different grids are examined and it is found that the 200 × 20 grid is able to provide grid-independent results. However, the 300 × 30 grid is used in the present numerical simulation.

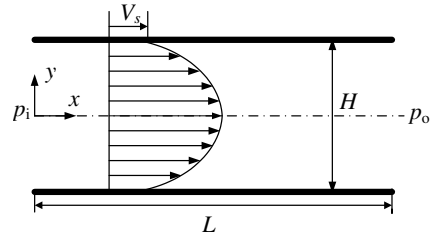

Fig. 1. Schematic of pressure-driven microchannel flow.

5. Results and discussions

Pong et al. [21] studied the pressure distributions along planar microchannels using an array of surface micromachined piezoresistive pressure sensors. In their experiments they found that pressure distributions are nonlinear in the microchannels due to compressibility. The computed pressure distributions along the stream-wise direction for nitrogen flow are compared with experimental results of Pong et al. in Fig. 2. Five inlet pressures are compared ($p_i =$ 135, 170, 205, 240 and 275 kPa). Our present numerical results agree very well with experimental data. When the pressure ratio is small, the effect of compressibility is small and the pressure gradient is almost constant. The trend towards a nonlinear distribution is clear when the pressure ratio becomes large.

The nitrogen gaseous flows and heat transfer at different *Kn* and *Re* are then studied. The length to height ratio (L/H) of the channel is 20 in the computation hereafter. The temperature of inlet gas is 300 K and the wall temperature is 400 K. The outlet pressure is 100 kPa, so the mean free path of nitrogen based on the outlet pressure and wall temperature at 400 K is 90.7 nm. The tangential momentum and thermal accommodation coefficients are set to unit in the present study. The variation of *Kn* is achieved by changing the channel height.

Slip velocities at the wall with and without thermal creep effect are first examined. From the results we find that thermal creep only affects the slip velocity at the entrance region. Because of the temperature difference between inlet gas and the wall, the tangential temperature gradients near the inlet is large and the thermal creep effect is obvious. As the fluid proceeding along the channel, the tangential temperature gradient decreases and so does the effect of thermal creep.

The axial variation of local Poiseuille number and local Nusselt number at different *Kn* is showed in Figs. 3 and 4, respectively. The Reynolds numbers in these cases are 2.2.

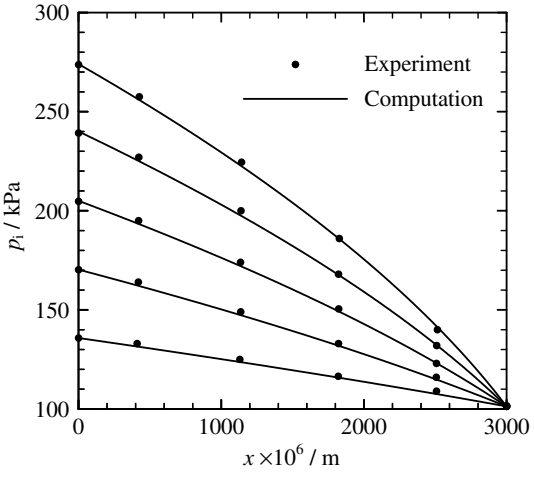

Fig. 2. Pressure distribution along the channel at five inlet pressures ($p_i = 135$, 170, 205, 240, and 275 kPa).

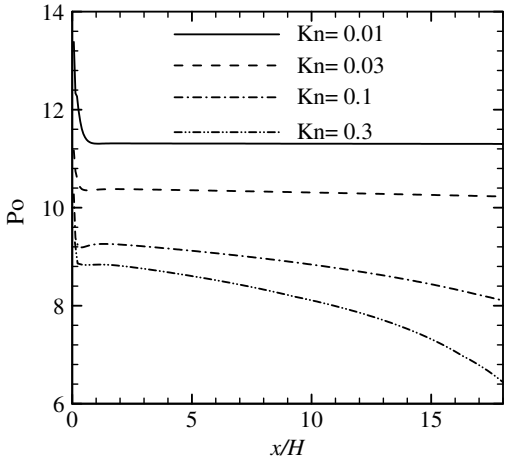

Fig. 3. Variation of *Po* along the channel at different *Kn*.

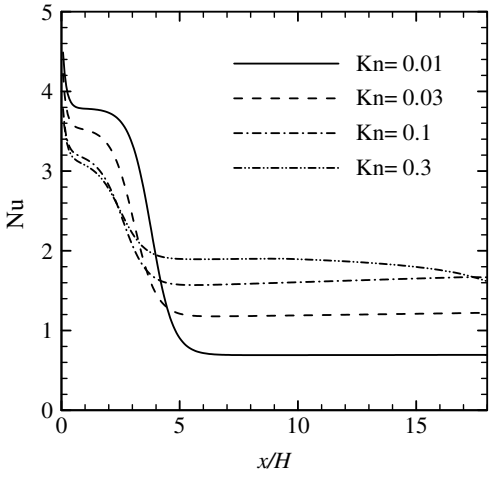

Fig. 4. Variation of *Nu* along the channel at different *Kn*.

Because of the difference in dimension, the inlet pressure is chosen to keep *Re* constant.

The local Poiseuille number decreases when proceeding along the channel. At small *Kn* (e.g., $Kn = 0.01$), *Po* decrease rapidly first near the inlet and then tends to a constant. But at large *Kn* (e.g., $Kn = 0.3$), *Po* decreases along the channel, not only in the entrance region, but in the whole channel. The fluid accelerates along the channel because of the density reduction brought about by the pressure drop. The normal velocity gradient at the wall also increases along the channel. The numerical results in Fig. 3 reveal that the increase in u outweighs the increase in normal velocity gradient when *Kn* is large.

Fig. 3 also demonstrates that the *Po* decreases with the increase of *Kn*. The velocity profile at larger *Kn* is flatter than that at smaller *Kn*. The normal velocity gradient at the wall decreases with the increase of *Kn* number. So the friction factor or the shear stress decreases with the increase of *Kn*.

From Fig. 4 we find that the distributions of local Nusselt number for compressible flow are different from those

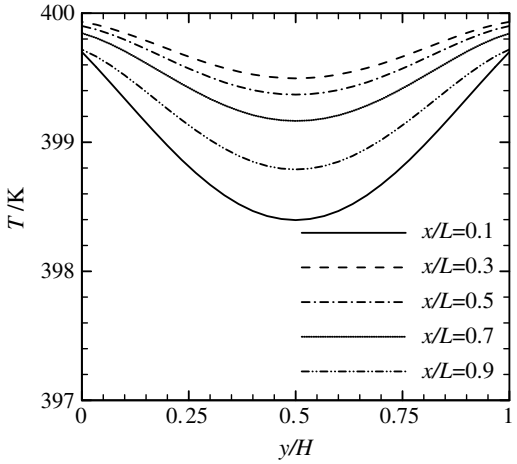

Fig. 5. Temperature profiles at different axial locations.

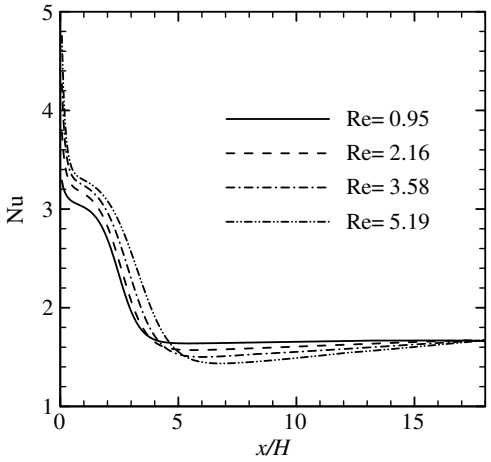

Fig. 7. Variation of *Nu* along the channel at different *Re*.

of incompressible flow. Similar *Nu* distributions are reported by in Chen [15] when studying steady compressible flow in microchannels.

When $Kn \leqslant 0.1$, *Nu* decreases rapidly first along the channel axis up to about $x/H = 5$, then it rises slowly afterwards. But when $Kn = 0.3$, *Nu* decreases along the whole channel. This peculiar behavior can be explained with the help of Fig. 5. $\frac{dT}{dn}\big|_w$ and $T_w - T_m$ both decrease rapidly near the inlet, but $\frac{dT}{dn}\big|_w$ decrease much more rapidly than $T_w - T_m$, so *Nu* decreases first. The fluid accelerates along the channel because of the density reduction brought about by the pressure drop. As the fluid velocity increases, more energy is transferred from the internal energy and flow work into the kinetic energy. As a result, the temperature decreases gradually. The largest temperature occurs at about $x/H = 2.2$. From this location afterward, $\frac{dT}{dn}\big|_w$ and $T_w - T_m$ increase gradually. When $Kn \leqslant 0.1$, the increase rate of $\frac{dT}{dn}\big|_w$ is larger that of $T_w - T_m$ when $x/H > 5$, so the *Nu* increases gradually. But for $Kn = 0.3$, the increase ratio of $\frac{dT}{dn}\big|_w$ is less than that of $T_w - T_m$, and *Nu* keeps on decreasing.

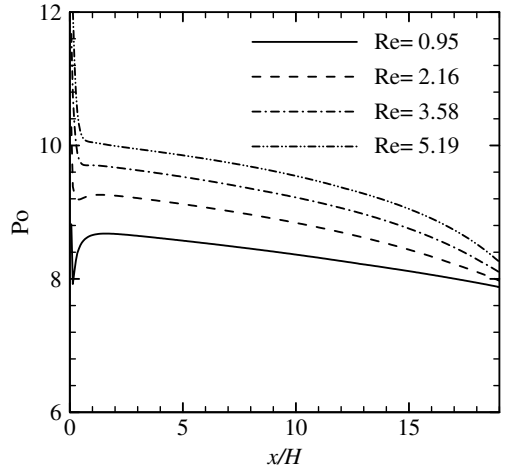

Fig. 6. Variation of *Po* along the channel at different *Re*.

The axial variation of local Poiseuille number and Nusselt number at different *Re* are demonstrated in Figs. 6 and 7, respectively. The *Kn* in these cases is 0.1. Fig. 6 depicts that the *Po* decreases when proceeding along the channel. There is a sudden reduction near the inlet when $Re = 0.95$ and 2.16. The local Poiseuille number increases as *Re* increases.

The effect of *Re* on local *Nu* distribution are not as obvious as that of *Kn*. Fig. 7 reveals that larger *Re* results in larger *Nu* when $x/H < 5$. The velocity-increase and temperature-drop along the channel due to expansion are more obvious at larger *Re*. Hence, the increase of *Nu* along the channel is also more obvious at larger *Re*.

6. Conclusions

The Augmented Burnett equations with slip boundary conditions are used to model the compressible gas flow and heat transfer in micro Poiseuille flow in slip and transition flow regime. The Burnett equations are numerically unstable at large Knudsen number. Convergent results could only be obtained when $Kn \leqslant 0.2$ in the past. The proposed relaxation method on the augmented Burnett terms enable us to obtain the convergent results up to $Kn = 0.4$, using 20 grids in the direction normal to the wall. From the computation we find that the stability of the Burnett equations is associated with grid Knudsen number. The critical Kn_{grid} number is about 8 according to our calculations. The thermal creep contribution on the slip velocity was taken into consideration in the simulation. The pressure distributions computed using the Burnett equations agree very well with experimental data.

With the increase of *Kn*, Poiseuille number decreases while Nusselt number increases. The local Poiseuille number decreases along the channel. At small *Kn* ($Kn = 0.01$), *Po* decreases rapidly first near the inlet and then tends to a constant value. But at larger *Kn*, *Po* decreases along the whole channel. The decrease is more obvious for larger *Kn*. When $Kn \leqslant 0.1$, the local Nusselt number decreases rapidly first along the channel axis, then it rises slowly

afterwards. But when $Kn = 0.3$, the local Nusselt decreases along the whole channel. This is a result of the competing effect of $\frac{dT}{dn}\big|_w$ and $T_w - T_m$.

The local Poiseuille number increases with the increase of *Re*. The decrease in Poiseuille number along the channel is more obvious at larger *Re*. The change in *Nu* along the channel is larger at larger *Re*.

Acknowledgement

This work was supported by the Major Program of the National Natural Science Foundation of China with Grant No. 10632070.

References

[1] J.C. Harley, Y. Huang, H.H. Bau, J.N. Zemel, Gas flow in micro-channels, J. Fluid Mech. 284 (1995) 257–274.
[2] M. Gad-el-Hak, The fluid mechanics of microdevices – the Freeman Scholar Lecture, Trans. ASME J. Fluid Eng. 121 (1999) 5–33.
[3] R.K. Agarwal, K.Y. Yun, R. Balakrishnan, Beyond Navier–Stokes: Burnett equations for flows in the continuum-transition regime, Phys. Fluids 13 (2001) 3061–3085.
[4] G.A. Bird, Molecular Gas Dynamics and the Direct Simulation of Gas Flows, Oxford University Press, 1994.
[5] S. Chapman, T.G. Cowling, The Mathematical Theory of Nonuniform Gases, Cambridge Univ. Press, New York, 1970.
[6] K.A. Fiscko, D.R. Chapman, Comparison of Burnett, super-Burnett, and Monte Carlo solutions for hypersonic shock structure, in: Proceedings of the 16th International Symposium on Rarefied Gas Dynamics, 1988, pp. 374–395.
[7] H. Xue, H.M. Ji, C. Shu, Prediction of flow and heat transfer characteristics in micro Couette flow, Microscale Thermophys. Eng. 7 (2003) 51–68.
[8] F.B. Bao, J.Z. Lin, Burnett simulation of flow and heat transfer in micro Couette flow using second-order slip conditions, Heat Mass Transfer 43 (2007) 559–566.
[9] O. Aydin, M. Avci, Analysis of laminar heat transfer in micro-Poiseuille flow, Int. J. Therm. Sci. 46 (2007) 30–37.
[10] N.G. Hadjiconstantinou, O. Simek, Constant-wall-temperature Nusselt number in micro and nano-channels, J. Heat Transfer 124 (2002) 356–364.
[11] M. Renksizbulut, H. Niazmand, G. Tercan, Slip-flow and heat transfer in rectangular microchannels with constant wall temperature, Int. J. Therm. Sci. 45 (2006) 870–881.
[12] Z.Y. Guo, X.B. Wu, Compressibility effect on the gas flow and heat transfer in a microtube, Int. J. Heat Mass Transfer 40 (1997) 3251–3254.
[13] Y. Asako, T. Pi, S.E. Turner, M. Faghri, Effect of compressibility on gaseous flows in micro-channels, Int. J. Heat Mass Transfer 46 (2003) 3041–3050.
[14] C.S. Chen, Numerical analysis of heat transfer for steady three-dimensional compressible flow in long microchannels, J. Enhanc. Heat Transfer 12 (2005) 171–188.
[15] D.A. Lockerby, J.M. Reese, High-resolution Burnett simulations of micro Couette flow and heat transfer, J. Comput. Phys. 188 (2003) 333–347.
[16] S. Colin, P. Lalonde, R. Caen, Validation of a second-order slip flow model in rectangular microchannels, Heat Transfer Eng. 25 (2004) 23–30.
[17] R.W. Barber, D.R. Emerson, Challenges in modeling gas-phase flow in microchannels: from slip to transition, Heat Transfer Eng. 27 (2006) 3–12.
[18] A. Beskok, G.E. Karniadakis, W. Trimmer, Rarefaction and compressibility effects in gas microflows, J. Fluid Eng-T ASME 118 (1996) 448–456.
[19] X. Zhong, Development and computation of continuum higher order constitutive relations for high-altitude hypersonic flow, Ph.D thesis, Stanford University, 1991.
[20] Y.C. Fang, Parallel simulation of microflows by DSMC and Burnett equations, Ph.D thesis, Western Michigan University, 2003.
[21] K.C. Pong, C.M. Ho, J.Q. Liu, Y.C. Tai, Non-linear pressure distribution in uniform micro-channels, Applications of Microfabrication to Fluid Mechanics, in: ASMEFED, vol. 197, 1994, pp. 51–56.